Journal of Sound and Vibration (1998) **215**(5), 1101–1120
Article No. sv981682

DYNAMIC DISPERSION CURVES FOR NON-HOMOGENEOUS, ANISOTROPIC BEAMS WITH CROSS-SECTIONS OF ARBITRARY GEOMETRY

V. V. Volovoi and D. H. Hodges
Georgia Institute of Technology, Atlanta, Georgia, U.S.A.

V. L. Berdichevsky
Wayne State University, Detroit, Michigan, U.S.A.

and

V. G. Sutyrin
Huntington Beach, California, U.S.A.

(*Received* 17 *September* 1997, *and in final form* 23 *March* 1998)

To accurately predict the dynamic behaviour of spanwise uniform, non-homogeneous, anisotropic beams with arbitrary cross-sectional geometry is an important part of engineering analysis. Classical one-dimensional beam theory fails in this endeavour, and development of more sophisticated one-dimensional theories is an important task. A basis for development of improved one-dimensional theory is the dispersion curve analysis. A means to find the dispersion curves is discussed in this paper. The code is developed to calculate the dispersion curves, as well as corresponding mode shapes. The code is based on finite element discretization over the cross-sectional domain. Use of this code provides benchmark results for the testing of any existing one-dimensional theory, as well facilitating the construction of new one-dimensional theories. Dispersion information can be also useful in non-destructive evaluation. As an example of a case where non-classical effects are particularly important, results obtained from this code for an I-beam are presented. Qualitative comparison with the well-known case of isotropic rectangular beam is provided. Features that are common for all beams are emphasized along with pointing out qualitative differences that exist for beams other than rectangular or circular.

1. INTRODUCTION

From the point of view of elastic wave propagation, prismatic beams represent waveguides, i.e. bodies with two or more parallel boundaries, that introduce one or more characterstic dimensions into the problem. This leads to a dependence of frequency on wave length for harmonic waves or *wave dispersion*. The equation describing this dependency is called the frequency or dispersion equation. There are two main reasons for obtaining dispersion information for beams:

(1) Any beam theory ought to provide a reasonable approximation for the dispersion relationships in order to capture the elastic behaviour of beams correctly. Thus, knowledge of the correct frequency spectra is crucial for the assessment of the validity of a beam theory for a given cross-sectional properties. For example,

0022–460X/98/351101 + 20 $30.00/0

quantification of the range of applicability of the St-Venant effect is readily provided.

(2) Dispersion information could be useful in its own right, e.g. when monochromatic stress waves are excited in beams, as in ultrasonic non-destructive evaluation. Sufficiently comprehensive information about the frequencies and mode shapes permits one to predict the reflection of such a stress wave from an end with various boundary conditions. This in turn provides tools for the development of a strategy for detection of defects in such beams by transmitting an optimal combination of waves that propagate along the beam and analysing the effects of their scattering due to the presence of defects.

The range of applicability of most existing one-dimensional (1-D) beam models in solving 3-D problems of dynamics of beams is restricted to the case of long waves ($a/l \ll 1$, $a \equiv$ the diameter of beam, $l \equiv$ the characteristic wavelength) and low frequencies ($(a\omega)/\sqrt{(G/\rho)} \ll 1$, $\omega \equiv$ characteristic frequency, $\rho \equiv$ density, $G \equiv$ characteristic elastic modulus). In many engineering problems, however, the need arises to study cases of high frequencies [$(a\omega)/\sqrt{(G/\rho)} \approx 1$] and short waves ($a/l \approx 1$). These limitations are especially stringent for composite beams. The term "classical beam theory" in the present work refers to the combination of Euler–Bernoulli theory for extension and bending and St-Venant theory for torsion.

The first dispersion equations for circular beams were obtained from 3-D elasticity by Pochhammer [1] and Chree [2], while the analogous problem for plates in plane strain was investigated by Rayleigh [3] and Lamb [4]. The discrepancy between the 3-D dispersion relationships and those given by classical beam theory prompted Rayleigh [5] to take into account the inertia of cross-sectional rotational motion in order to improve the dispersion equation given by classical beam theory. Love [6] later derived beam equations of motion with the Rayleigh correction. Note that an approximated theory given by Chree [2], where the Bessel functions were replaced by the first two terms in their power expansion, yielded results that are practically identical to the Rayleigh frequency equation. Timoshenko [7] then generalized classical 1-D beam theory by introducing shear deformation. Timoshenko theory provided better correlation with experimental data, particularly for the dynamics of beams. The removal of the Kirchhoff assumption and introduction of the new degree of freedom associated with rotation of a cross section permitted the modeling of the first flexural thickness shear mode for long waves, i.e. the lowest high-frequency mode for circular cross sections (see for example reference [8]). Still, the correlation with 3-D elasticity was poor for some other cross sections (especially for open ones). Moreover, even for circular or rectangular cross sections, it was not clear how to model other high-frequency modes, nor how to describe the short-wave effects.

The next step for construction of an improved 1-D theory was accomplished by Mindlin and his collaborators. Logically it could be traced from the derivation of Mindlin's first-order shear deformation theory for plates [9], where the so-called "cut-off" frequency, i.e. the non-zero frequency of thickness-shear motions corresponding to very long waves, was matched with the values given by the Rayleigh–Lamb solutions of 3-D elasticity. Recall that Reissner's approach to the same problem [10, 11] involved an assumed stress distribution and application of a complimentary variational principle without consideration of dynamics. Both approaches provided remarkably close values for the shear correction factor ($\pi^2/12$ and $5/6$ respectively). It is noted that the Mindlin approach was extended recently to laminated anisotropic shells and plates in reference [12].

The first approximate theory to take into account the coupling between longitudinal and radial modes in a circular cylinder with free lateral surfaces was constructed in reference

[13]. Later, a three-mode system of 1-D equations was derived in reference [14] for axially symmetric motions of an elastic rod of circular cross section. A new mode called "axial shear" was introduced therein that was fully coupled with two modes from reference [13]. This additional mode had a dominant axial displacement field that was quadratically distributed in the radial direction and had one circular nodal line at $r = a/2$, where a is radius of the cross section and r is the radial coordinate. The following technique was used to obtain 1-D equations. The displacement field was expanded in terms of Jacobi polynomials in the radial direction. Three 1-D variables, called potential functions, ϕ_i, were introduced, these satisfy the Helmholtz equations, so that the displacement field can be expressed in terms of ϕ_i. In addition, four correction factors were introduced, which were used to match the cut-off frequencies and curvatures at cut-off of the axial shear and radial modes as derived from both approximate and exact theories. It was shown in reference [15] that the resulting 1-D model correctly described waves reflected from the free end due to the incident extensional wave. For a narrow band of frequencies this incident wave gives rise to a standing wave with decreasing amplitude away from the beam end. This phenomenon was called "end resonance" and was observed experimentally in reference [16]. A comprehensive numerical study by using a collocation method of these curves was given in references [17, 18]. Later, the three-mode theory was extended to transversely isotropic circular cylinders in references [19] and [20].

The underlying idea promoted by Mindlin and his followers for the development of approximate theories was the following: 1-D beam theory should give a satisfactory description of the wave propagation in an infinite beam, and the main dynamic characteristics of an infinite beam are reflected in the behaviour of the dispersion curves. Therefore, once a way to accurately approximate the dispersion curves is found, a simplified model of beams based on this approximation can be created. Only by succeeding in that task could one expect a reasonable agreement between 3-D elasticity and a corresponding 1-D beam model. A similar conclusion has been reached independently and almost simultaneously in the physics of solids, where analysis of dispersion curves of crystalline bodies was employed to improve classical elasticity theory (see a comprehensive review in the monograph by Kunin [21]).

1.1. USE OF A 2-D FINITE ELEMENT DISCRETIZATION OVER THE CROSS SECTION

Apparently, finite element discretization over the cross-section of a beam for calculation of the dispersion relationships was employed for the first time in reference [22]. Methodology for obtaining dispersion curves for the propagating modes (i.e. modes for which the wave numbers are real) for arbitrary cross-sectional geometry was presented therein, along with the examples of both isotropic as well as orthotropic square cross section.

The complete set of dispersion curves including the "evanescent" branches (i.e. those which pertain to complex wave numbers) was calculated using 1-D finite elements for circular anisotropic cylinders and composite plates in references [23] and [24], respectively. A slightly different 1-D finite element formulation which maintains continuity of not only displacements by tractions as well was used first for plates in reference [25] and then for circular cylinders in reference [26]. This approach leads to a generalized eigenvalue problem of fourth order and it is advantageous for recovering stress fields corresponding to the modes of vibrations.

2-D finite elements were used to study decaying modes in static behaviour of beams in references [27] and [28]. Both works contained open cross section examples with the latter work focusing on the restrained torsion problem. Borri and his collaborators (see references [29] and an extension of that work to initially twisted beams [30]) studied the

statics of anisotropic beams with basic equations being derived from the virtual work principle. Evanescent static modes (or ''extremity solutions'' as they were referred in those works) were also studied therein.

In reference [31] a quadratic eigenvalue problem was considered that is identical to the one studied in the present paper. Wave reflection from the free end was studied therein, and examples with rectangular cross sections were presented. Later, pretwist was included in the formulation, and its influence was studied in the examples of and rectangular cross sections [32]. The work of Hladky-Hennion [33] was focused on circular waveguides, i.e. when waves propagate in the circumferential direction. Triangular and rectangular cross sections were considered therein. The procedure was similar to the one employed in reference [34]. The latter work was restricted to thin-walled beams and shell theory was used. In both works displacements along the axial coordinate were assumed to be shifted by a phase of $\pi/2$ compared to the other two displacements. That leads to an eigenproblem with real symmetric matrices in the isotropic case. It is important to recognize, however, that this procedure provides no advantage for studying general anisotropic beams (see the discussion below). In reference [35] sets of dispersion branches for real wave numbers were presented for an orthotropic rectangular cross section.

Finally, as an illustration of application of the dispersion curves let us note [36] where the eigenfunctions were first obtained either by the so-called propagator matrix approach [37] (for laminated isotropic cylinders) or using finite elements in the radial direction [23] (for anisotropic cylinders). Then the expansion with respect to these eigenfunctions was used to evaluate the complex amplitudes as well as the energy flux associated with the reflected waves at the free end of the cylinder. This evaluation was conducted using both variational and least-square methods and the former technique was found to be superior.

This brief overview of the relevant literature is intended to demonstrate that, while the need for dispersion information was appreciated by many authors, to our knowledge prior to this work dispersion curves were studied almost exclusively for rectangular or circular cross sections, while dispersion information for other important sectional geometries remains very scarce. The intent of the present paper is to demonstrate fundamental differences in the topology of the dispersion curves for various cross sections. Further, the connection of these differences to various refinements of classical beam theory and the range of validity of classical theory itself are discussed. Intended applications of the developed tools include capabilities to analyse with high precision complicated composite cross sections such as realistic helicopter rotor blades, which places stringent requirements on the versatility of the code. Therefore, it is deemed appropriate to describe in sufficient detail the algorithm which satisfies those requirements and allows calculation of dispersion information for a wide range of frequencies and wave numbers.

2. PRESENT APPROACH

Let us consider an infinite prismatic beam that occupies a domain

$$\Omega = \{-\infty < x_1 < \infty, (x_2, x_3) \in S\}$$

with some prescribed cross section S, and where x_1, x_2, x_3 are Cartesian coordinates so that x_1 is aligned with the beam axis; $\partial\Omega$ is the boundary of Ω. The following procedure which leads to a quadratic generalized problem is pretty standard, so it will be covered very briefly. Notations are taken from references [38] and [39] with the differences

emphasized herein. The variational formulation of the 3-D elasticity problem requires minimization of the following functional per unit length:

$$2\mathscr{I} = \langle \Gamma^T D \Gamma \rangle - \langle \rho \dot{v}^T \dot{v} \rangle, \tag{1}$$

whre v is the 3-D vector of displacements, dots refer to time derivatives, $\langle \cdot \rangle$ to integration over the cross section, D is the 6×6 matrix of material coefficients, ρ is density and $\Gamma = \lfloor \Gamma_{11}, 2\Gamma_{12}, 2\Gamma_{13}, \Gamma_{22}, 2\Gamma_{23}, \Gamma_{33} \rfloor^T$ is the 6×1 strain matrix that can be split into two parts:

$$\Gamma = \Gamma_h v + \Gamma_l v', \tag{2}$$

where prime refers to the partial derivative with respect to axial coordinate, while Γ_l and Γ_h have the form

$$\Gamma_h = \begin{bmatrix} 0 & 0 & 0 \\ \frac{\partial}{\partial x_2} & 0 & 0 \\ \frac{\partial}{\partial x_3} & 0 & 0 \\ 0 & \frac{\partial}{\partial x_2} & 0 \\ 0 & \frac{\partial}{\partial x_3} & \frac{\partial}{\partial x_2} \\ 0 & 0 & \frac{\partial}{\partial x_3} \end{bmatrix}, \qquad \Gamma_l = \begin{bmatrix} 1 & 0 & 0 \\ 0 & 1 & 0 \\ 0 & 0 & 1 \\ 0 & 0 & 0 \\ 0 & 0 & 0 \\ 0 & 0 & 0 \end{bmatrix}. \tag{3}$$

The Cauchy conditions at $t = 0$ need not be specified at this stage of derivation, and the lateral surfaces of the beam are considered to be free of tractions.

Due to the fact that properties of prismatic beams do not depend on the axial coordinate x_1, fundamental beam solutions have the form

$$\tilde{v}(x_2, x_3)\, \mathrm{e}^{(ikx_1 - \omega t)}, \tag{4}$$

where k and ω are wavenumber and frequency, respectively. These fundamental solutions can be found by minimizing the complex functional

$$2\tilde{\mathscr{I}} = \langle \tilde{v}^T (\Gamma_h^T - ik\Gamma_l^T) D (\Gamma_h + ik\Gamma_l) \tilde{v} \rangle - \omega^2 \langle \rho \tilde{v}^T \tilde{v} \rangle. \tag{5}$$

A nontrivial solution of this problem exists only for particular values of k and ω. We refer to such values, plotted in the space of k and ω, as dispersion curves and to the continuous pieces of them as branches. It is convenient to use 2-D plots with the left part reserved for $\mathfrak{F}(k)$ and the right part for $\Re(k)$. (Due to the intrinsic symmetry of the problem explained below, both these quantities can be considered positive without a loss of generality; see Figure 1.) Branches with complex k are then depicted by two curves, one in the left of the plot and one in the right. The corresponding set of eigenfunctions comprises an infinite-dimensional basis for beam solutions. Discretization over the cross section allows for the representation of the displacement field

$$\tilde{v}(x_2, x_3) = S(x_2, x_3) V. \tag{6}$$

Here, S is a $3 \times N$ matrix of shape functions, and V is N-dimensional vector of nodal displacements. Substitution of equations (4) and (6) into equation (5) yields

$$2\tilde{\mathscr{I}} = V^T (E - ikE_l + k^2 D_{ll} - \omega^2 M) V, \tag{7}$$

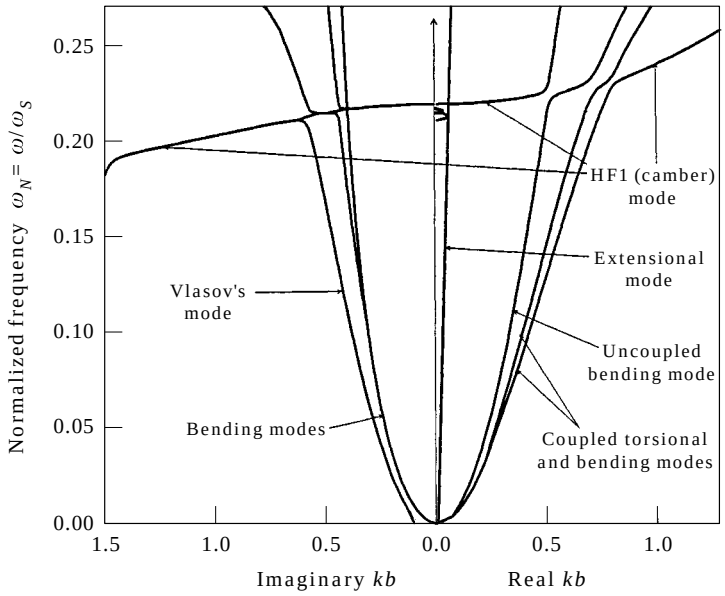

Figure 1. Dispersion curves (frequency spectrum) for anisotropic I-beam, 960 6-noded elements.

where symmetric matrices E, D_{ll}, M, and the skew-symmetric matrix E_l are given by

$$E = \langle [\Gamma_h S]^T D \Gamma_h S \rangle, \qquad E_l = \langle [\Gamma_h S]^T D \Gamma_l S \rangle - \langle [\Gamma_l S]^T D \Gamma_h S \rangle,$$
$$D_{ll} = \langle [\Gamma_l S]^T D \Gamma_l S \rangle, \qquad M = \langle \rho S^T S \rangle. \tag{8}$$

All these matrices are readily available from VABS [40], a 2-D finite element code that uses 6- and 8-noded isoparametric elements.

Extraction of the fundamental solution in the form equation (4) is equivalent to the eigenvalue problem

$$(E - ikE_l + k^2 D_{ll} - \omega^2 M)\tilde{v} = 0. \tag{9}$$

Many authors (see, for example, references [33] and [34]) slightly altered equation (4) looking instead for a solution of the form

$$\begin{Bmatrix} \hat{v}_1 \\ \hat{v}_2 \\ \hat{v}_3 \end{Bmatrix} = \begin{Bmatrix} i\tilde{v}_1 \\ \tilde{v}_2 \\ \tilde{v}_3 \end{Bmatrix}. \tag{10}$$

This is certainly advantageous for isotropic materials. As shown in Appendix A this leads to the eigenvalue problem

$$(\hat{E} + k\hat{E}_l + k^2 \hat{D}_{ll} - \omega^2 \hat{M})\hat{v} = 0, \tag{11}$$

where all participating matrices are real and symmetric. Moreover, all propagating modes (i.e. eigenvectors corresponding to real k) are also real. However, for a general anisotropic material this is not always the case (see Appendix A and also the discussion on the related issue pertaining to anisotropic plates [41]). Before proceeding with the description of the numerical procedure, let us point out some symmetry properties of equation (9).

(1) If k is an eigenvalue with the right eigenvector u, then by taking the complex conjugate of the both sides of equation (9) it becomes evident that $-\overline{k}$ is also an eigenvalue with the right eigenvector $\bar{u}$.

(2) If k is an eigenvalue with the right eigenvector u, then the transposition of the equation leads to the conclusion that $-k$ is also an eigenvalue with the left eigenvector u^T.
(3) Combination of the previous two properties renders $\bar{k}$ being an eigenvalue of the problem if k is an eigenvalue.

It is convenient to introduce "state space" notation:

$$P \equiv \begin{bmatrix} 0 & I \\ -D_{II} & E_I \end{bmatrix}, \qquad Q \equiv \begin{bmatrix} I & 0 \\ 0 & S \end{bmatrix}, \tag{12}$$

$$\lambda \equiv \frac{1}{ik}, \qquad z \equiv \begin{Bmatrix} iku \\ u \end{Bmatrix}, \tag{13}$$

where $S \equiv \omega^2 M - E$, and I is the identity matrix. Then

$$Pz_i = \lambda_i Q z_i \tag{14}$$

poses a standard generalized eigenproblem that is equivalent to the one given by equation (9). Let us note that at this point the matrix Q is real and symmetric, but it is not positive definite. Although this problem can be solved directly, there is one generic problem for all iterative procedures of finding eigenvalues that rely on Krylov's subspace concept: unless the eigenvector associated with the largest eigenvalue is eliminated it will inevitably corrupt the calculation of the smaller eigenvalues. In the case considered the elimination of the largest eigenvalue was not feasible. Moreover, due to the above-mentioned intrinsic symmetry problem, even fewer distinct eigenvalues can be recovered. All these problems can be bypassed by introducing a shift into the complex plane of k.

A complex shift allows one to look for k in any specified region of a complex plane in the neighborhood of a "guess" k_0, so that

$$k = k_0 + \tilde{k}. \tag{15}$$

Casting our eigenvalue problem in terms of $\tilde{k}$ we can represent it in a form which is similar to the original problem, with new complex matrices $\tilde{D}_{II}$, $\tilde{E}_I$, $\tilde{S}$:

$$\tilde{D}_{II} \equiv D_{II}, \qquad \tilde{E}_I \equiv E_I - 2ik_0 D_{II}, \qquad \tilde{S} \equiv k_0^2 D_{II} + ik_0 E_I - S. \tag{16}$$

The fact that in this case we have to operate with complex matrices does not constitute an insurmountable obstacle, and a straightforward generalization of two-sided Lanczos recursion to the complex variables was then implemented. On the elementary level of the computer simulation for a given ω, and a guess for k we calculated the k closest in the complex plane to the guess. Precision usually decreases if the initial guess is at approximately the same distance (or far away) from the two closest roots. In this case the guess has to be changed appropriately. It is interesting to note that precision also decreases if the initial guess is too close to the exact root, which results in ill-conditioned matrices.

In light of the above the following algorithm is used for obtaining a full picture of dispersion curves:

(1) *Determining the intersections of the dispersion curves with the plane* $\omega = 0$. For zero ω we make several initial guesses for k in a desired region of complex plane of k. Those guesses should cover this region sufficiently densely to avoid skipping a branch.

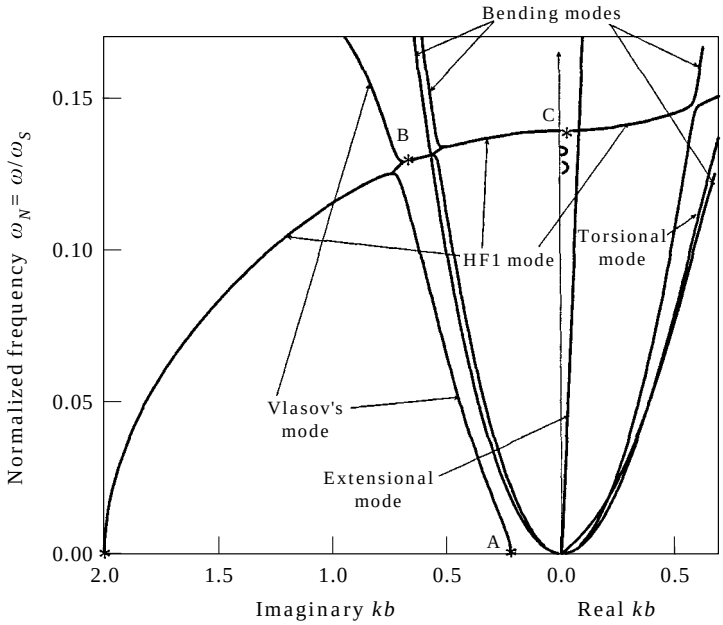

Figure 2. Dispersion curves (frequency spectrum) for an isotropic I-beam, 960 6-noded elements.

(2) *Improving the accuracy of calculation of the starting point*. This is done by adjusting the initial guesses (using results of step 1). The starting points of the branches are then determined.
(3) *Continuing the branches*. Each branch requires a separate iterative procedure that starts from the points obtained in step 2. We appropriately increment ω and find

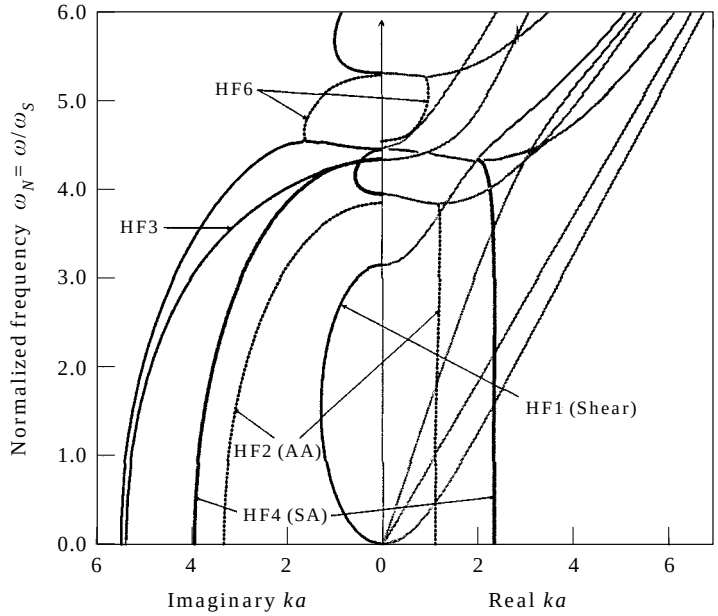

Figure 3. Dispersion curves (frequency spectrum) for an isotropic square cross section, 400 6-noded elements.

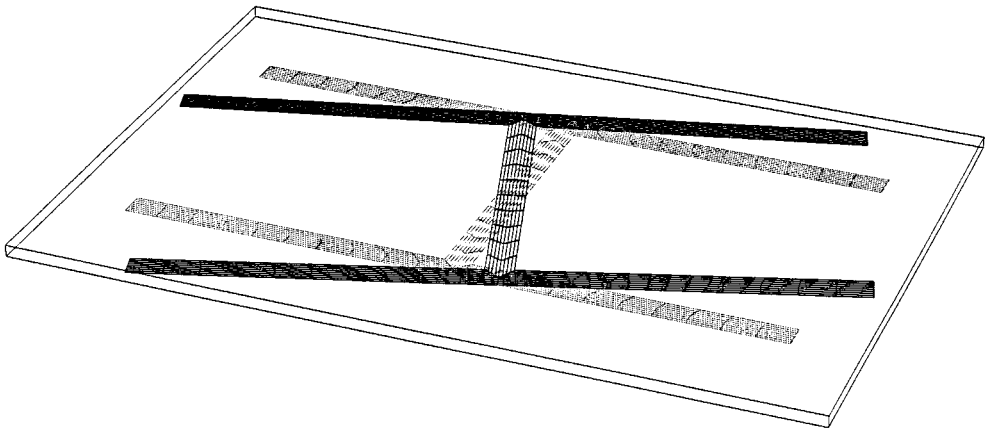

Figure 4. First "non-classical" (Vlasov) mode for isotropic I-beam: $\mathfrak{F}(bk) = 0{\cdot}2283$, $h/b = 0{\cdot}04$.

the corresponding k, thus following the branch into the region of high frequency ω. Intersections of branches require special monitoring (see below).

The eigenvector for each eigenvalue obtained allows us to recover the corresponding mode shape, i.e. the acutal 3-D distribution of the displacements for a given cross section. The constructed mode shape helps to ensure that we are not jumping from one branch to another (since branches located even very closely to each other possess very different mode shapes). The relative error, as a result of back-substitution of the calculated eigenvector into the original problem, is typically of the order 10^{-7} or even lower.

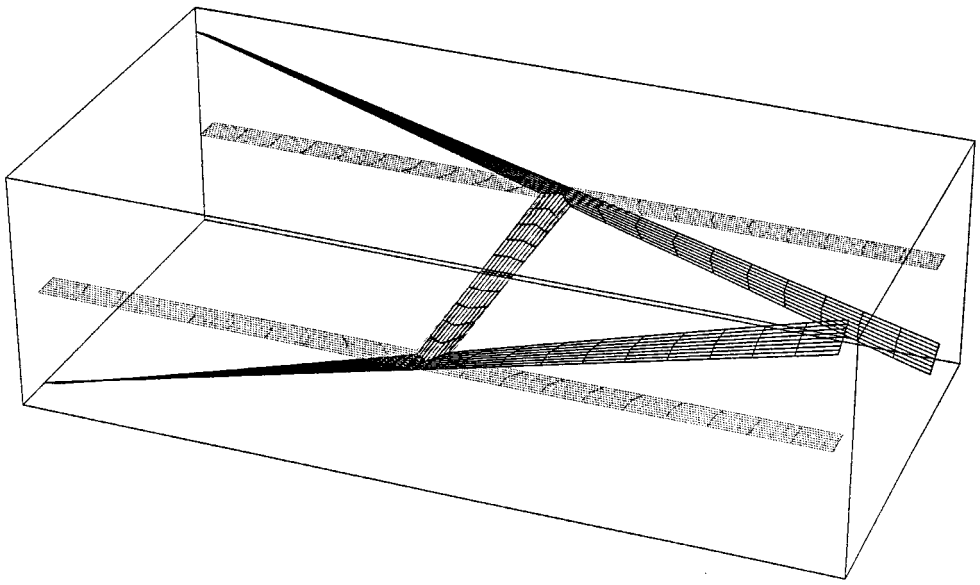

Figure 5. Scaled up out-of-plane part of a first "non-classical" (Vlasov) mode for isotropic I-beam.

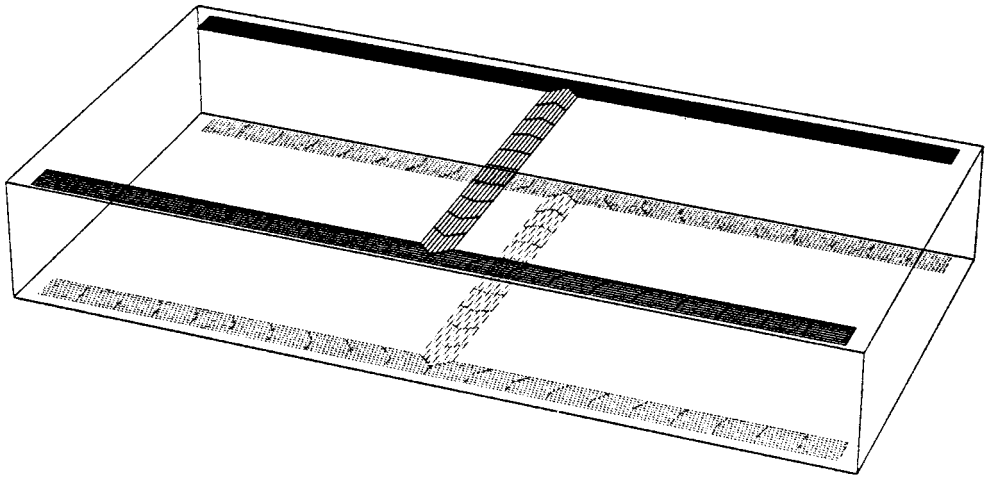

Figure 6. "Main" part of the extensional mode for antisymmetric I-beams.

3. RESULTS AND DISCUSSION

In the beginning of this section certain features of the dispersion sets that are common for all beams are described. This provides a convenient interpretation of the classical beam theory. Next, low frequency propagating modes of vibration are considered in some detail to emphasize the differences and similarities for isotropic and anisotropic beams. Finally, specific examples of the dispersion sets are presented and connections between various cross sectional properties and improved 1-D theories are investigated.

3.1. CONNECTION TO CLASSICAL THEORY

Figures 1, 2, and 3 depict typical sets of dispersion curves. For all these sets for small ω, there are only four real values of k representing an "interior" stress state which is described by classical beam theory. For $\omega = 0$ (statics), all these branches converge to point $k = 0$, which corresponds to the vicinity of the origin. All other values of k are complex, and $\mathfrak{F}(k)$ has the sense of a decay rate from the left end of the beam if $\mathfrak{F}(k) > 0$, and from the right end otherwise. There are only two such branches that emanate from the origin into the area of purely imaginary k. They correspond to the hyperbolic part of bending motion and can be represented either by Euler–Bernoulli or Timoshenko theories. Thus, the classical theory of beams with free lateral surfaces can be viewed as a truncated representation of the displacement field by the use of the first four of the basis eigenfunctions. It is "exponentially" exact for small ω in the sense that all corrections stem from the end effects, which decay exponentially as they penetrate in the interior of the beam. This observation naturally provides the range of validity for a classical theory: ω has to be smaller than the first cut-off frequency, since otherwise another propagating mode must be taken into consideration. This cut-off frequency, generally speaking, is of order $(\sqrt{G/\rho})/a$ (see below for discussion on variation of this frequency for different cross sections) which explains the limits mentioned in the introduction part.

There is one subtlety here that needs to be pointed out. In statics there are 12 zero roots for k in equation (9). However, there are only 4 distinct eigenvectors (modes) corresponding to those roots: three translations and torsional rotation of a cross section as a rigid body. In particular, 2 rotations of a cross section associated with bending do not constitute those modes. This can be shown first by noting that for $k = 0$ from equation (9) an eigenvector should belong to the null space of E. This matrix is associated with

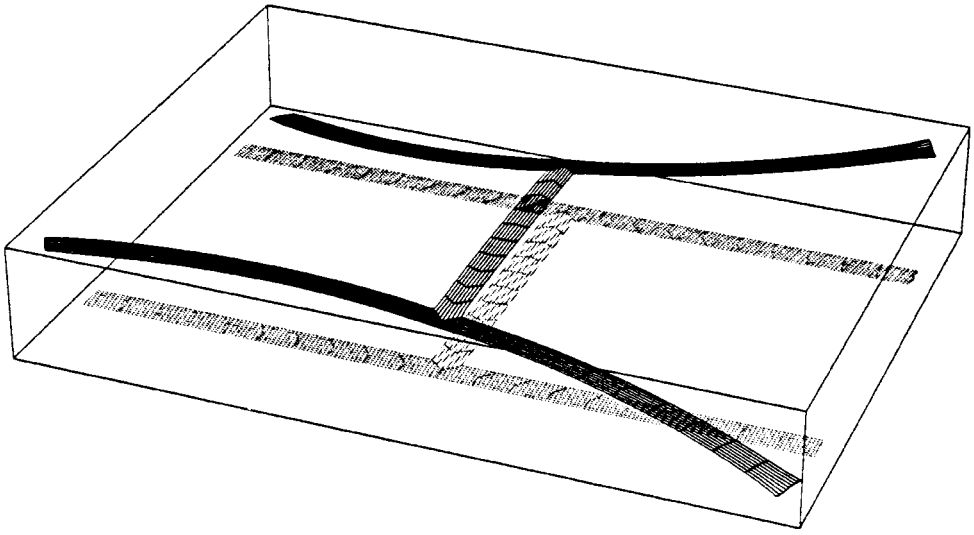

Figure 7. Scaled up "correction" part of the extensional mode for antisymmetric I-beams.

strains in the cross section alone, so that displacements in axial direction do not affect those strains. This in turn can be visualized as a projection of the 3-D displacement field of the cross section onto the cross section itself. Then it becomes clear that rotation of a cross section associated with bending will result in a "shrinking" of the projection, which will clearly entail non-zero strains.

It is also noteworthy to mention that, as can be observed from equation (9) for purely imaginary k, eigenvectors are real as long as $E - \omega^2 M$ is a positive definite matrix. In particular this is always true in statics ($\omega = 0$).

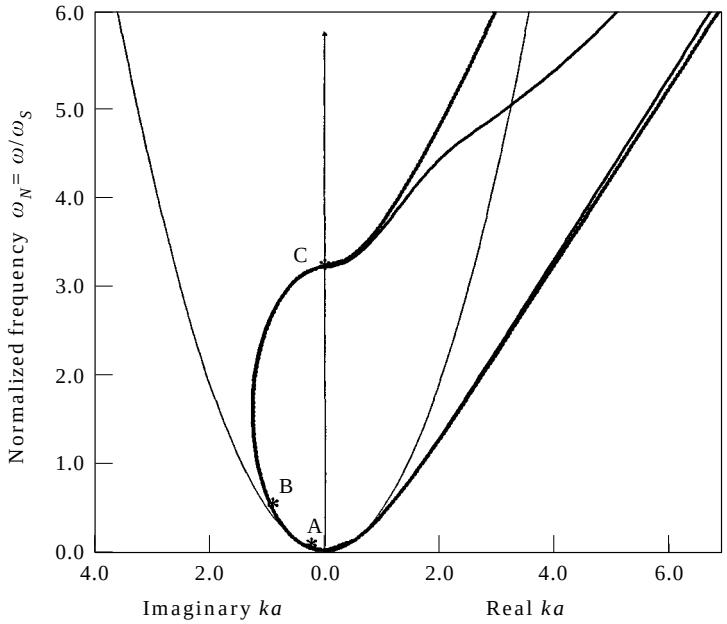

Figure 8. Dispersion curve for bending of square isotropic beam $\nu = 0{\cdot}3$: ——, 3-D simulations; ——, Timoshenko; - - - , Euler–Bernoulli.

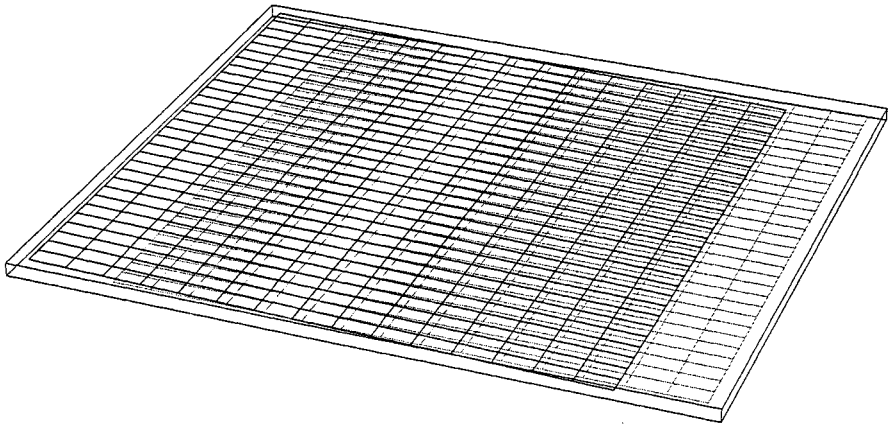

Figure 9. "Shear mode" for a square cross section: point A, $\omega = 0{\cdot}01$.

3.2. PROPERTIES OF CLASSICAL MODES

It is instructive to explore the shapes of the classical branches. Note that for non-zero values of ω, even for real k, the eigenvector is complex, with real and imaginary parts contributing in the opposite phase. Thus, we actually have modes with two connected parts. For isotropic beams real and imaginary parts reflect a separation of pure in-plane warping from out-of-plane warping (the latter are scaled up). In classical theory this phase shift is manifested in the fact that if the "main" part of the displacement has magnitude $\Psi(x_1)$ (e.g. θ for torsion or w for bending) then a "correction" would have magnitude $\Psi'(x_1)$ (θ' for the magnitude of St-Venant warping and w' for the rotation of a cross section in accordance with Kirchhoff hypothesis, respectively). A bending mode for isotropic I-beams is shown in Figures 12 and 13, while a torsional mode is shown in Figures 14 and 15. This provides a physical motivation for casting the problem in the form of equation (11). Corresponding eigenvectors are assumed to be real in this case, which implies that axial displacements are always out of phase with in-plane displacements. (The formulae in Appendix A demonstrate range of the validity of this assumption; in particular it is perfectly valid for isotropic beams.) Consequently, for isotropic beams this approach (see

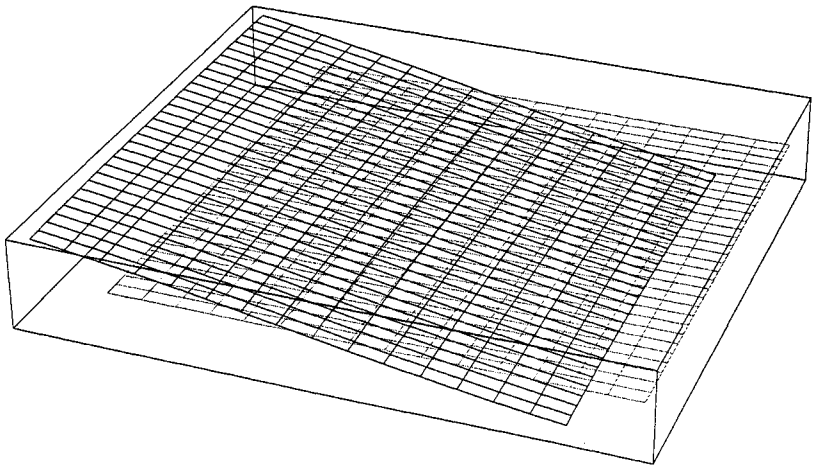

Figure 10. "Shear mode" for a square cross section: point B, $\omega = 0{\cdot}5$.

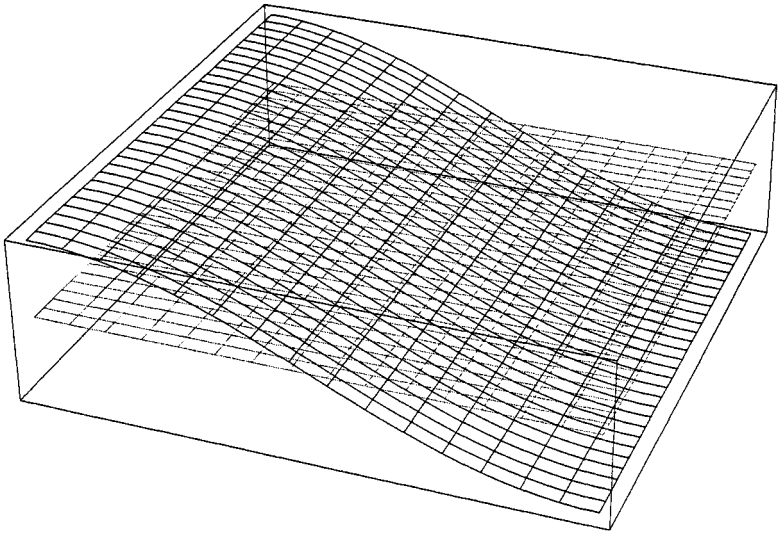

Figure 11. "Shear mode" for a square cross section: point C, $\omega = \pi$.

reference [34]) provides satisfactory results. The difference of less than 10% for propagating modes can be easily explained by the thin shell approximation employed in that paper. However, let us note in passing that even in this case the statement made in the cited paper that these modes do not deform the cross section is incorrect. In addition, this method of reference [34] does not provide any advantage for studying evanescent modes, which are crucial for thin-walled, open cross sections as discussed below.

For anisotropic beams the situation is different altogether. The mode shapes of the low frequency vibrations become coupled, and each mode is a combination of bending, torsion and extension. For example, if we consider beams with twist-extension coupling (antisymmetric beams) then this difference of in-plane and axial motions in phase will be violated as can be clearly observed studying two portions of the mode for I-beams with antisymmetric layup in Figures 6 and 7. As an example we consider an I-beam depicted in Figure 17, where angle plies on the flanges are taken to be the same $\theta = 20^\circ$ for both lower and upper flanges. This illustrates the importance of the terms that are neglected by restricting consideration to equation (11). Those neglected terms are written explicitly in Appendix A.

3.3. SPECIFIC EXAMPLES OF DISPERSION CURVES

For illustrative and verification purposes the dispersion curves for rectangular cross sections were obtained. (See Figure 3; cf. reference [32] where only pure imaginary or pure real wave numbers are displayed.) Next, the code was applied to I-beams. This choice was motivated by the well-recognized importance of non-classical effects for this case, as well as the existence of Vlasov's theory. This theory is known to give satisfactory results at least for thin-walled, isotropic beams with open cross sections (for general discussion of the generalization of the Vlasov's theory to anisotropic beams see reference [42]). Frequency is normalized with respect to $\omega_s = \sqrt{G/a^2\rho}$ where a and G are characteristic cross-sectional dimension and elastic shear modulus, respectively. This normalization is traditional and stems from the analysis of waves in isotropic bodies. Let us note, however, that for anisotropic analysis this normalization can be somewhat misleading, and the actual values of ω_s can be much smaller than for isotropic materials.

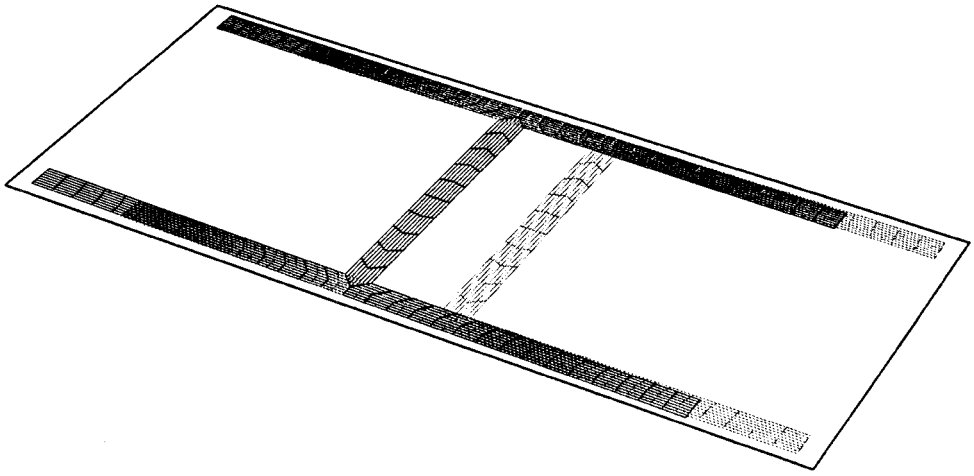

Figure 12. "Main (inplane) part of a bending mode shape for isotropic I-beams.

The I-beam first studied has a symmetric cross section and is made from graphite-epoxy material with a $[0^\circ/90^\circ]_4$ layup in the web and a $[(0^\circ/90^\circ)_3/(\theta)_2]$ in the flanges (see Figure 17). Geometry is defined by the following ratios $a/b = 0{\cdot}5$ and $h/b = 0{\cdot}04$, where constants a, b and h are the height of the web, the width of the flanges, and the thickness, respectively. Dispersion curves depicted in Figure 1 are for the case $\theta = 15^\circ$ For comparison, an isotropic beam of the same geometry has been studied, and Figure 2 depicts dispersion curves for Poisson's ratio $v = 0{\cdot}42$.

For a rectangular cross section high frequency (HF) branches are enumerated in order of ascending cut-off frequencies. Note that HF2 (corresponding mode shape is

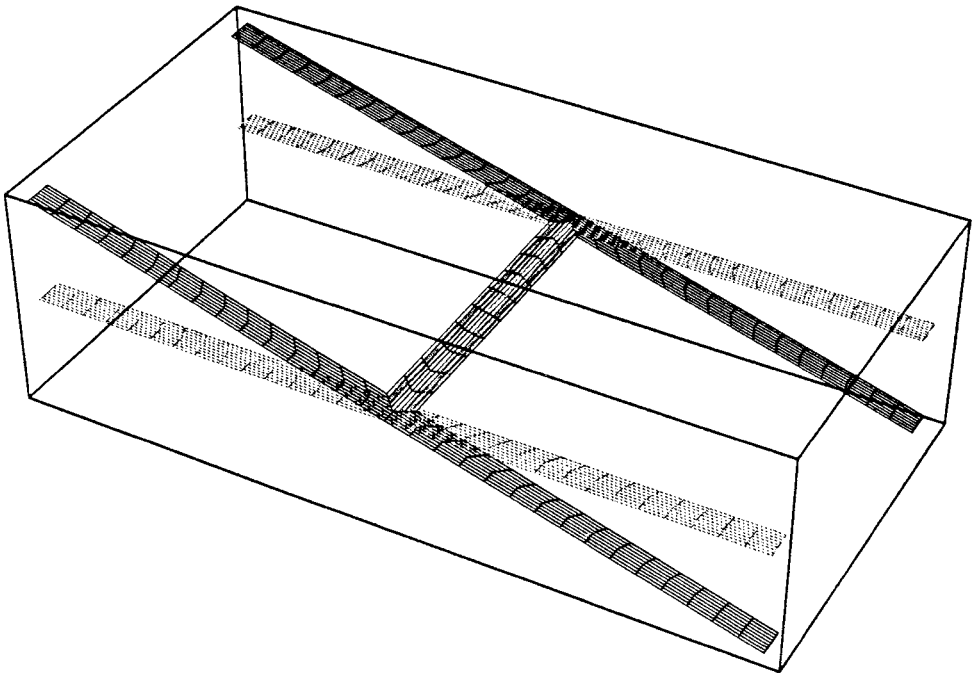

Figure 13. Scaled up "correction" (out-of-plane) part of a bending mode shape for isotropic I-beams.

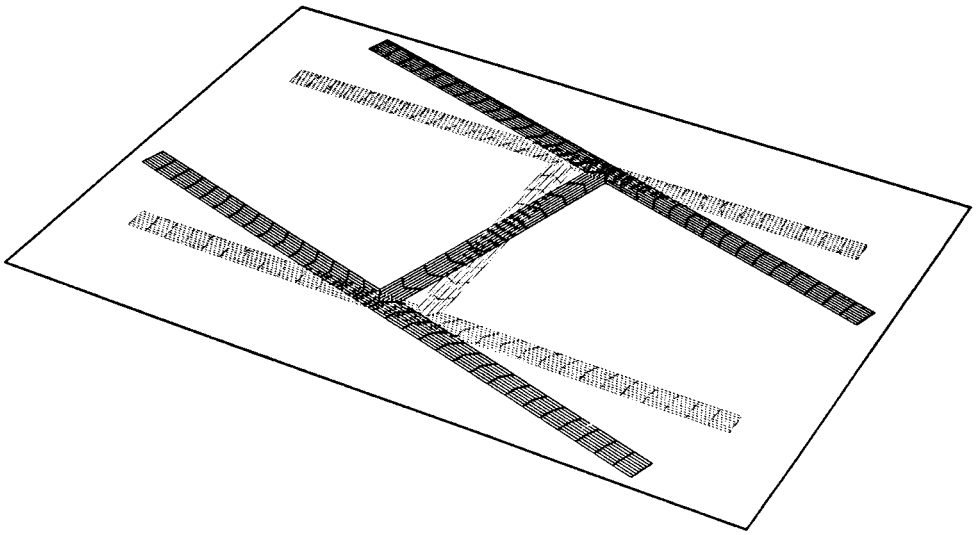

Figure 14. "Main" (inplane) part of a torsional mode shape for isotropic I-beams.

antisymmetric with respect to both cross-sectional axis of symmetry), HF4 (corresponding mode shape is antisymmetric with respect to one of the cross-sectional axis of symmetry, and symmetric with respect to the other), and HF6 are neither purely real nor purely imaginary for low frequencies. Since the cross section is square, HF1 and HF4 are "double" branches when one mode shape can be obtained from the other by a rotation by $\pi/2$. Similarly, two propagating modes (i.e. modes with real k) that correspond to bending in two orthogonal directions are depicted by two coinciding branches.

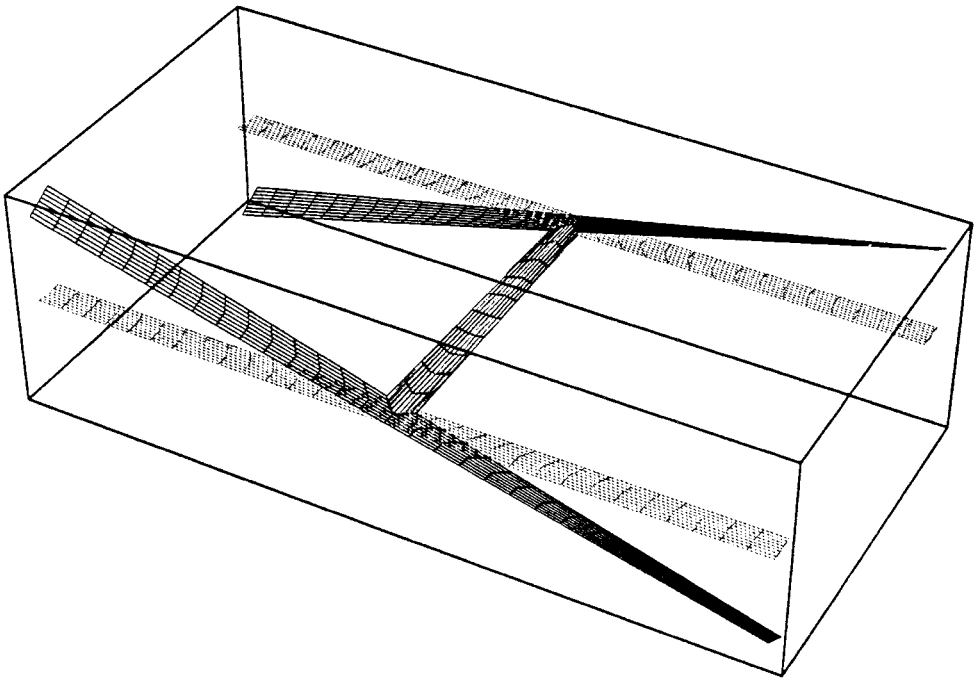

Figure 15. Scaled up "correction" (out-of-plane) part of a torsional mode shape for isotropic I-beams.

3.4. DIFFERENCES IN THE DISPERSION SETS DUE TO VARIOUS GEOMETRIES OF THE CROSS SECTIONS

Let us compare Figures 1 and 2 with Figure 3. In the latter case HF1 corresponds to shear deformation and is effectively a bending mode which "strayed" from the hyperbolic path predicted by the Euler–Bernoulli theory (see Figure 8 for comparison of the dispersion curves). It is remarkable how the shape of the corresponding mode changes with the frequency: for low frequency ($\omega_N = 0{\cdot}01$—point A in Figure 8) the dominant part of the mode is transverse translation of the cross section as a rigid body, which is the same motion that characterizes the mode for a real k (Figure 12). This is exactly the assumption of the Euler–Bernoulli theory. However, for a slightly higher frequency ($\omega_N = 0{\cdot}5$—point B in Figure 8) rotation of a cross section becomes visible (see Figure 9). This rotation is in agreement with the Euler–Bernoulli theory—the relative amplitude of the rotation is effectively proportional to $\mathfrak{F}(k)$, but the cross section begins to warp. Finally in the vicinity of cut-off frequency $\omega_N = \pi$ (see point C in Figure 8) shear deformation of the cross section is clearly observed Figure 10 and Euler–Bernoulli theory is invalid. This illustrates the importance of Timoshenko theory for solid cross sections.

For open cross sections, however, this high frequency branch is relatively unimportant since there are other more significant effects: there is an evanescent branch stemming from point A on Figure 2 with very slow decay rate that certainly has to be taken into consideration. Hence, one sees the importance of Vlasov's theory [43]. The mode shape of this crucial mode (see Figure 4; cf. Figure 14) remarkably coincides with the torsional displacement of a cross section which is in full agreement with Vlasov's theory. The same holds for out-of-plane warping (see Figure 5; cf. Figure 15). Of course, for purely imaginary k both portions of the mode are in phase; i.e. the eigenvector is real. Moreover, excellent quantitative correlation for the decay rate as provided by Vlasov's theory was observed. Similar observation had been also made in reference [28] where wide flange and angle sections were considered. A detailed asymptotic study of Vlasov's theory [42] provided a solid mathematical foundation for this coincidence as well as a consistent generalization of Vlasov's theory for the anisotropic case.

In addition to the "Vlasov" mode a different motion corresponding to the HF1 mode can be important for higher frequencies. This relates to the fact that this different mode of vibration starts to penetrate deeper into the interior of the beam, until finally (point C on Figure 2) the branch crosses the $k = 0$ axis, and the corresponding vibrations cease to decay at all. Figure 16 depicts the shape of this eigenfunction ("camber" mode). Let

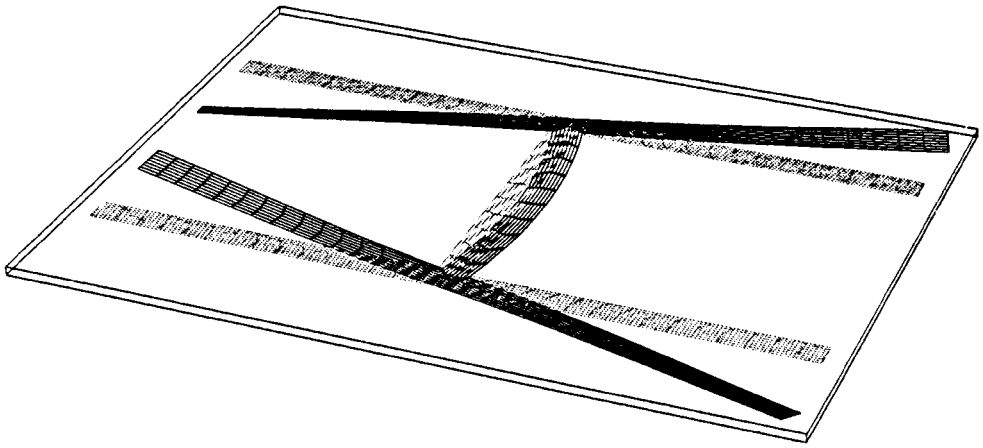

Figure 16. Second "non-classical" (camber) mode for isotropic I-beam: $\mathfrak{F}(bk) = 1{\cdot}9996$, $h/b = 0{\cdot}04$.

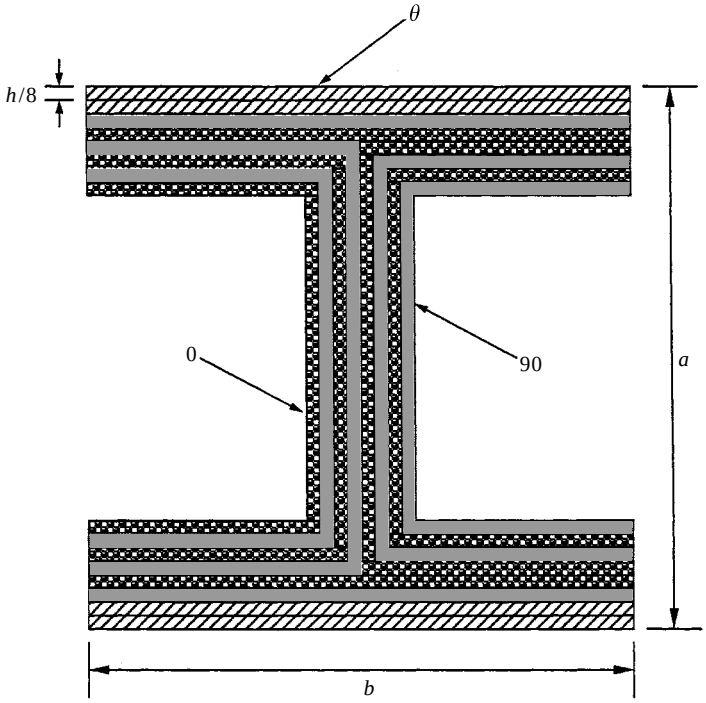

Figure 17. Lay-up of anisotropic I-beams.

us note that this cut-off frequency can be two orders of magnitude less than the lowest cut-off frequency for solid isotropic beams.

The examples considered illustrate a direct connection of the requirements for a refined beam theory with the properties of the dispersion curves associated with a given cross section. In particular, for open thin-walled cross sections the Timoshenko correction is relatively unimportant, and other modes of vibrations, such as Vlasov and camber ones, need to be considered first.

4. CONCLUDING REMARKS

A method for calculation of dispersion curves is presented. This method has been extensively correlated with results existing in the literature. New results for both isotropic and anisotropic I-beams are presented. Currently there is no doubt that dispersion curves help to elucidate the physical behaviour of beam dynamics. The topology of the dispersion curves strongly depends on the geometry and material properties of the beam cross section. Thus, various non-classical effects have different relative importance for various beams. This information can be used to determine which of the non-classical modes of vibration are the most influential for a given beam. This would, in turn, pave the way for the development of a new 1-D theory that would be capable of adequately approximating solutions of the dynamic 3-D elasticity of beams.

REFERENCES

1. L. POCHHAMMER 1876 *Zeitschrift für reine angewandte Mathematik* **81**, 324–336. Über die Fortpflanzungsgeschwindigkeiten kleiner Schwingungen in einem unbegrenzten isotropen Kreiszylinder.

2. C. Chree 1886 *Quarterly Journal of Pure and Applied Mathematics* **24**, 287–298. On the longitudinal vibrations of a circular bar.
3. Lord Rayleigh 1889 *Proceedings of the London Mathematical Society* **10**, 225–234. On the free vibrations of an infinite plate of homogeneous isotropic elastic matter.
4. H. Lamb 1917 *Proceedings of the London Mathematical Society*, *Series A* **93**, 114–128. On waves in an elastic plate.
5. Lord Rayleigh 1949 *Theory of Sound*. New York: Macmillan: volume 1, 2nd edition.
6. A. E. H. Love 1944 *Mathematical Theory of Elasticity*. New York: Dover; 4th edition.
7. S. Timoshenko 1922 *Philosophical Magazine*, *Series* 6 **43**, 125–131. On the transverse vibration of bars of uniform cross sections.
8. J. Miklowitz 1978 *Elastic Waves and WaveGuides*. Oxford: North-Holland.
9. R. D. Mindlin 1951 *Journal of Applied Mechanics* **18**, 31–38. Influence of rotary inertia and shear on flexural motion of isotropic, elastic plates.
10. E. Reissner 1945 *Journal of Applied Mechanics* **12**, A69–A77. The effect of transverse shear deformation on the bending of elastic plates.
11. E. Reissner 1947 *Quarterly Journal of Applied Mathematics* **5**, 55–68. On bending of elastic plates.
12. S. B. Dong and C. K. Chun 1992 *Journal of Applied Mechanics* **59**, 372–379. Shear constitutive relations for laminated anisotropic shells and plates: Part I—methodology.
13. R. D. Mindlin and G. Herrmann 1951 *Proceedings of the First U. S. National Congress of Applied Mechanics*, Ann Arbor. A one-dimensional theory of compressional waves in an elastic rod; 187–191.
14. R. D. Mindlin and H. D. McNiven 1960 *Journal of Applied Mechanics* **27**, 152–158. Axially symmetric waves in elastic rods.
15. H. D. McNiven 1961 *The Journal of the Acoustical Society of America* **33**, 23–27. Extensional waves in a semi-infinite elastic rod.
16. J. Oliver 1957 *The Journal of the Acoustical Society of America* **26**, Elastic wave dispersion in a cylindrical rod by a wide-band short-duration pulse technique.
17. J. Zemanek 1962 *Ph.D. dissertation*, *University of California at Los Angeles*. An experimental and theoretical investigation of elastic wave propagation in a solid cylinder.
18. J. Zemanek 1972 *The Journal of Acoustical Society of America* **51**, 265–283. An experimental and theoretical investigation of elastic wave propagation in a solid cylinder.
19. H. McNiven and Y. Mengi 1969 *The Journal of the Acoustical Society of America* **49**, 230–236. Dispersion of waves in transversely isotropic rods.
20. Y. Mengi and H. D. McNiven 1971 *The Journal of the Acoustical Society of America* **50**, 248–257. Axially symmetric waves in transversely isotropic roads.
21. I. Kunin 1982 *Theory of Elastic Media with Microstructure*. Berlin: Springer; volume, 1 and 2.
22. B. Aalami 1973 *Journal of Applied Mechanics* **40**, 1067–1072. Waves in prismatic guides of arbitrary cross section.
23. H. K. Huang and S. B. Dong 1984 *Journal of Sound and Vibration* **96**, 363–379. Propagating waves and edge vibrations in anisotropic composite cylinders.
24. S. B. Dong and K. H. Huang 1985 *Journal of Applied Mechanics* **52**, 433–438. Edge vibrations in laminated composite plates.
25. S. K. Datta, A. H. Shah, R. L. Brattan and T. Chakraborty 1989 *Journal of Acoustical Society of America* **83**, 2020–2026. Wave propagation in laminated composite plates.
26. N. Rattanawangcharoen, A. H. Shah and S. K. Datta 1992 *International Journal of Solids and Structures* **29**, 767–781. Wave propagation in laminated composite circular cylinders.
27. D. B. Goetschel and T. H. Hu 1985 *Computers and Structures* **21**, 869–874. Quantification of Saint-Venant's principle for a general prismatic member.
28. M. Kazic and S. B. Dong 1990 *Journal of Engineering Mechanics* **116**, 870–891. Analysis of restrained torsion.
29. V. Giavotto, M. Borri, P. Mantegazza, G. Ghiringhelli, V. Carmaschi, G. C. Maffuoli and F. Mussi 1983 *Computers and Structures* **16**, 403–413. Anisotropic beam theory and applications.
30. M. Borri, G. L. Ghiringhelli and T. Merlini 1992 *Composites Engineering* **2**, 433–456. Linear analysis of naturally curved and twisted anisotropic beams.
31. S. B. Dong and M. Kazic 1989 *Vibration Analysis—Techniques and Application*, 12*th Biennial Conference on Mechanical Vibration and Noise*; Montreal. ASME. End modes and their application to wave reflection analysis. DE-Vol. 18-4, 199–208.

32. O. Onipede Jr and S. B. Dong 1996 *Journal of Sound and Vibration* **195**, 313–330. Propagating waves and end modes in pretwisted beams.
33. A. C. Hladky-Hennion 1996 *Journal of Sound and Vibration* **194**, 119–136. Finite element analysis of the propagation of acoustic waves in waveguides.
34. L. Gavrić 1994 *Journal of Sound and Vibration* **173**, 113–124. Finite element computation of dispersion properties of thin-walled waveguides.
35. T. Mazúch 1996 *Journal of Sound and Vibration* **198**, 429–438. Wave dispersion modelling in anisotropic shells and rods by the finite element method.
36. N. Rattanawangcharoen, A. H. Shah and S. K. Datta 1994 *Journal of Applied Mechanics* **61**, 323–329. Reflection of waves at the free edge of a laminated circular cylinder.
37. W. M. Karunasena, A. H. Shah and S. K. Datta 1991 *International Journal of Solids and Structures* **27**, 949–964. Reflection of plane strain waves at the free edge of a laminated composite plate.
38. V. V. Volovoi 1997 *Ph.D dissertation*, *Aerospace Engineering*, *Georgia Institute of Technology*. On end effects in prismatic beams.
39. C. E. S. Cesnik, V. G. Sutyrin and D. H. Hodges 1996 *International Journal of Solids and Structures* **33**, 1387–1408. Refined theory of twisted and curved composite beams: the role of short-wavelength extrapolation.
40. C. E. S. Cesnik and D. H. Hodges 1997 *Journal of the American Helicopter Society* **42**, 27–38. VABS: a new concept for composite rotor blade cross-sectional modeling.
41. S. B. Dong and K. E. Pauley 1978 *Journal of the Engineering Mechanics Division* **104**, 801–817. Plane waves in anisotropic plates.
42. V. V. Volovoi, D. H. Hodges, V. L. Berdichevsky and V. Sutyrin 1998 *International Journal of Solids and Structures*. Asymptotic theory for static behavior of elastic anisotropic I-beams. In press.
43. V. Z. Vlasov 1961 *Thin-Walled Elastic Beams*. National Science Foundation and Department of Commerce.

APPENDIX A: EXPLICIT COEFFICIENTS OF EQUATION (11)

The following is the derivation of explicit coefficients for equation (11) if the unknown variables are represented in the form of equation (10). Let $\hat{S}$ denote shape functions for node m before the assembly, and consider the contribution to strain energy part in the functional (5) only from that node:

$$V_m^T \hat{S}(\Gamma_h^T - ik\Gamma_l^T) D(\Gamma_h + ik\Gamma_l)\hat{S}V_m, \tag{A1}$$

where Γ_h and Γ_l are provided by equation (2) and (3) respectively, $D \equiv [d_{ij}]$ is the 6×6 matrix of material coefficients, and V_m is the vector of nodal displacements. Using displacements in the form of equation (10), we can rewrite the strains:

$$\hat{\Gamma}_h \hat{S} = \begin{bmatrix} 0 & 0 & 0 \\ i\hat{S}_{,2} & 0 & 0 \\ i\hat{S}_{,3} & 0 & 0 \\ 0 & \hat{S}_{,2} & 0 \\ 0 & \hat{S}_{,3} & \hat{S}_{,2} \\ 0 & 0 & \hat{S}_{,3} \end{bmatrix}, \qquad i\Gamma_l \hat{S} = \hat{S} \begin{bmatrix} -1 & 0 & 0 \\ 0 & i & 0 \\ 0 & 0 & i \\ 0 & 0 & 0 \\ 0 & 0 & 0 \\ 0 & 0 & 0 \end{bmatrix}, \tag{A2}$$

where commas denote partial derivatives with respect to coordinates in the cross-sectional plane. Substituting equation (A2) into equation (A1) renders the following expression for the contribution into the coefficients of the equations (11) from the considered node (for convenience real and imaginary parts are separated):

Appendix A—(*Continued on following page*)

$$\Re[\hat{E}_m] = \begin{bmatrix} d_{22}\hat{S}_{,2}^2 + 2d_{23}\hat{S}_{,2}\hat{S}_{,3} + d_{33}\hat{S}_{,3}^2 & 0 & 0 \\ 0 & d_{44}\hat{S}_{,2}^2 + 2d_{25}\hat{S}_{,2}\hat{S}_{,3} + d_{55}\hat{S}_{,3}^2 & d_{45}\hat{S}_{,2}^2 + (d_{46} + d_{55})\hat{S}_{,2}\hat{S}_{,3} + d_{56}\hat{S}_{,3}^2 \\ 0 & d_{45}\hat{S}_{,2}^2 + (d_{46} + d_{55})\hat{S}_{,2}\hat{S}_{,3} + d_{56}\hat{S}_{,3}^2 & d_{55}\hat{S}_{,2}^2 + 2d_{56}\hat{S}_{,2}\hat{S}_{,3} + d_{66}\hat{S}_{,3}^2 \end{bmatrix}, \tag{A3}$$

$$\Im[\hat{E}_m] = \begin{bmatrix} 0 & -d_{24}\hat{S}_{,2}^2 - (d_{25} + d_{34})\hat{S}_{,2}\hat{S}_{,3} - d_{35}\hat{S}_{,3}^2 & -d_{25}\hat{S}_{,2}^2 - (d_{26} + d_{35})\hat{S}_{,2}\hat{S}_{,3} - d_{36}\hat{S}_{,3}^2 \\ d_{24}\hat{S}_{,2}^2 + (d_{25} + d_{34})\hat{S}_{,2}\hat{S}_{,3} + d_{35}\hat{S}_{,3}^2 & 0 & 0 \\ d_{25}\hat{S}_{,2}^2 + (d_{26} + d_{35})\hat{S}_{,2}\hat{S}_{,3} + d_{36}\hat{S}_{,3}^2 & 0 & 0 \end{bmatrix}, \tag{A4}$$

$$\Re[\hat{E}_{lm}] = \hat{S}\begin{bmatrix} 0 & (d_{22} - d_{14})\hat{S}_{,2} + (d_{23} - d_{15})\hat{S}_{,3} & (d_{23} - d_{15})\hat{S}_{,2} + (d_{33} - d_{16})\hat{S}_{,3} \\ (d_{22} - d_{14})\hat{S}_{,2} + (d_{23} - d_{15})\hat{S}_{,3} & 0 & 0 \\ (d_{23} - d_{15})\hat{S}_{,2} + (d_{33} - d_{16})\hat{S}_{,3} & 0 & 0 \end{bmatrix}, \tag{A5}$$

$$\Im[\hat{E}_{lm}] = \hat{S}\begin{bmatrix} 0 & 0 & 0 \\ 0 & 0 & -[(d_{25} - d_{34})\hat{S}_{,2} + (d_{26} - d_{35})\hat{S}_{,3}] \\ 0 & [(d_{25} - d_{34})\hat{S}_{,2} + (d_{26} - d_{35})\hat{S}_{,3}] & 0 \end{bmatrix}, \tag{A6}$$

$$\Re[\hat{D}_{llm}] = \hat{S}^2\begin{bmatrix} d_{11} & 0 & 0 \\ 0 & d_{22} & d_{23} \\ 0 & d_{23} & d_{33} \end{bmatrix}, \qquad \Im[\hat{D}_{llm}] = \hat{S}^2\begin{bmatrix} 0 & -d_{12} & -d_{13} \\ d_{12} & 0 & 0 \\ d_{13} & 0 & 0 \end{bmatrix}. \tag{A7}$$

Note: For isotropic beams all imaginary parts vanish.